Title
DIAGNOSIS AND CORRECTION OF BEAM BEHAVIOR IN AN ISOCHRONOUS CYCLOTRON

Authors
Garren, Alper A.
Smith, Lloyd.

Publication Date
1963-04-02

University of California

Ernest O. Lawrence Radiation Laboratory

Berkeley, California

UCRL-10756
c.2

DISCLAIMER

UCRL-10756

UNIVERSITY OF CALIFORNIA

Lawrence Radiation Laboratory
Berkeley, California

Contract No. W-7405-eng-48

DIAGNOSIS AND CORRECTION OF BEAM BEHAVIOR IN AN ISOCHRONOUS CYCLOTRON

Alper A. Garren and Lloyd Smith

April 2, 1963

DIAGNOSIS AND CORRECTION OF BEAM BEHAVIOR IN AN ISOCHRONOUS CYCLOTRON

Alper A. Garren and Lloyd Smith

Lawrence Radiation Laboratory
University of California
Berkeley, California

April 2, 1963

ABSTRACT

A description is given of methods used to observe phase behavior, orbit centering, and oscillation amplitude and frequencies in a cyclotron. These methods are being used to facilitate development of new 88-inch-cyclotron beams. Beam properties are deduced from the intensity as a function of radius, probe shadows, 3-finger and "C"-probe measurements. Required corrections make use of calculations based on magnet measurements.

DIAGNOSIS AND CORRECTION OF BEAM BEHAVIOR IN AN ISOCHRONOUS CYCLOTRON*

Alper A. Garren and Lloyd Smith

Lawrence Radiation Laboratory
University of California
Berkeley, California

April 2, 1963

DETERMINATION AND CORRECTION OF BEAM PHASE

Since the 88-inch cyclotron does not yet have a reliable phase probe, we have developed a method for determining the beam phase distribution as a function of radius by analysis of beam intensity vs. radius (I vs. R) measurements on an ordinary probe for a range of dee frequencies.

We note first that, apart from an additive constant, the sine of the phase lag for all particles in the beam is the same function of radius. Specifically, the phase lag ϕ is given by

$$\sin\phi(R) \approx \sin\phi(0) - 2\pi \frac{mc^2}{\Delta E} \left(\frac{\omega}{c}\right)^2 \left[\int_0^R \frac{\Delta B(R)}{B_s(0)}\, R\, dR - \frac{\Delta\omega}{\omega} \frac{R^2}{2}\right], \qquad (1)$$

where $\Delta B(R)$ is the departure of the actual magnetic field from the synchronous field $B_s(R)$, $\Delta\omega$ is the departure of the frequency from the value ω corresponding to B_s, and ΔE is the peak energy gain per turn. The procedure is to determine the ΔB contribution to $\sin\phi$ by systematic variations of the known $\Delta\omega$ term.

Suppose, for example, that the beam phase behavior for the reference frequency is as shown in Fig. 1(a). Each solid curve shows the phase history of a representative particle in the beam. The resultant I vs. R curve [Fig. 1(b)] shows constant intensity to radius A, where some particles begin

to be decelerated; decreasing intensity to radius B; constant intensity to radius C; and the final decrease to zero intensity at radius D. If the frequency is decreased, the curves of Fig. 1(a) are shifted downward by an amount proportional to $R^2\Delta\omega$, causing points A and B to move inward, and C and D to move outward in radius by amounts uniquely determined by the shape of the $\sin\phi$ curves of Fig. 1(a). At the same time the intensity in the plateau between B and C decreases, eventually reaching zero when the uppermost phase curve of Fig. 1(a) is depressed to -1 at B. On the other hand, increasing the frequency causes points A and B to move outward, and C and D inward. Eventually the dip at A will disappear. At some positive frequency shift two new intensity break points will appear at smaller radii as the inner maximum exceeds $\sin\phi = +1$.

Because of the unique relation between the I vs. R and the $\sin\phi(R)$ curves, the phase curves for a reference frequency may be deduced from a set of I vs. R measurements at different frequencies by subtracting the appropriate frequency-shift contributions to $\sin\phi$ at the break points from ± 1. Moreover, from the shape of the I vs. R curves between break points like A and B one can deduce the phase distribution of the beam.

A typical set of such measurements taken from a 130-MeV α-particle beam is shown in Fig. 2 (cleaned up to show relevant features). The intensity losses were shown to arise from lack of synchronism, rather than axial losses, by observing that no current appeared on a stationary probe above and below the median plane (C-probe) as the moving probe was withdrawn. The phase diagram deduced from these curves is shown in Fig. 3. The crosses mark points which were predicted by computer programs that used measured iron and trim-coil fields. It should be remarked that such detailed information

about beam phase behavior requires a high degree of stability of frequency and magnetic field, since frequency shifts of 1 kc cause significant changes in the I vs. R curves.

The phase widths of beams we have analyzed are 40 to 50 deg, and the distribution seems to be peaked towards the phase-lagging side, which is reasonable for the source-puller geometry used.

Improvement of beam phase behavior, if indicated, is obtained from computed curves showing the contribution of each trim coil (or set of trim coils connected in series) to $\sin\phi(R)$; see Fig. 4. Since these trim-coil effects are rather flat out to the coil radius, they make a contribution to $\sin\phi$ quadratic in radius, as does the frequency-shift term. Consequently, simultaneous tuning of a trim coil and the dee frequency can make a phase correction starting near one of the undesirable peaks or valleys of the $\sin\phi$ curves. Though this correction will continue out to larger radii, trim coils farther out can compensate. In this way one can systematically straighten out the phase curves.

BEAM CENTERING

A convenient way to determine if the beam is centered is to place the three probes (120 deg apart) at the same radius. The beam is centered if, and only if, each probe picks up the same amount of beam.

The beam may be centered by changes of dee voltage and source-puller geometry, by tuning with the first-harmonic correction coils in the valleys, or both. While the first method is most useful for getting the beam centered at all radii, it is harder than the second method, which generally suffices to center the beam near the coupling resonance radius and deflector entrance.

VERTICAL STABILITY

The most useful instrument for detecting axial loss has been the so-called C-probe, which extends above and below the median plane, over a large radial range. By watching C-probe current vs. radius on another probe one can determine the radii where axial loss occurs.

The effect of the trim coils on axial stability is conveniently displayed by use of curves of the contribution to ν_z^2 of each trim-coil power supply; namely, the contribution to $\mu' = (R/B)(dB/dR)$. These are shown in Fig. 5 for the 130-MeV α case. One must take care that the μ' changes from the trim coils do not cause vertical instability.

RADIAL-AMPLITUDE DETERMINATION

The amplitude of incoherent radial oscillations may be deduced from measurements of the radial extent of the shadow cast by one probe on another. We have worked out a graphical method for predicting such shadow shapes, similar to that used for predicting deflector transmission efficiency.[1]

Consider two probes, an upstream one at radius R_1 and zero azimuth, a downstream one at radius R_2 and azimuth $\theta_2 < \pi$. Suppose a particle has radial amplitude A, phase ϕ and equilibrium orbit radius on the zeroth turn (we may label turns arbitrarily) $r_{0eq} = R_1 - A - \lambda\Delta r$, where Δr is the turn separation and λ, $0 \leq \lambda \leq 1$, is a random variable expressing the assumption that the radial density distribution is uniform. On the kth turn the radius of this particle at azimuth θ will be

$$r_k(\theta) = R_1 + (k - \lambda)\Delta r - A\left\{1 - \cos\left[\nu_r\theta - \phi + 2\pi(\nu_r - 1)k\right]\right\}, \qquad (2)$$

where ϕ, λ are random variables within the limits

$$0 \leq \phi \leq 2\pi, \qquad 0 \leq \lambda \leq 1. \qquad (3)$$

A particle will strike the upstream probe if there is some turn number n such

that $r_k(0) < R_1$ and $r_k(\theta_2) < R_2$ for all $k < n$, and $r_n(0) \geq R_1$; otherwise, it will strike the downstream probe. These conditions may be written

$$\left.\begin{aligned} &1 - \cos(\phi - k\Delta) > (k - \lambda)\,\Delta r/A \\ &(R_2 - R_1)/A + \left[1 - \cos(\phi - k\Delta - \nu_r\theta_2)\right] > (k - \lambda)\,\Delta r/A \end{aligned}\right\} \text{ all } k < n$$
$$1 - \cos(\phi - n\Delta) \leq (n - \lambda)\,\Delta r/A \ , \qquad (4)$$

where $\Delta = 2\pi(\nu_r - 1)$ and ϕ, λ obey (3). The construction is illustrated in Fig. 6 for a particular choice of θ_2, ν_r, and $\Delta r/A$. For each choice of $\Delta r/A$ one gets a different angle α and consequently a different curve 3, showing the range of phases hitting each probe. Such a sequence is shown in Fig. 7, which corresponds to $\nu_r\theta_2 = 120$ deg. Each curve encloses the phases striking probe 2 as a function of $(R_2 - R_1)/A$. These curves are labeled by their values of A/A_0, where $A_0 = \Delta r/2\pi(\nu_r - 1)$. For a low-energy cyclotron $\nu_r \approx 1$ and we will introduce little error by replacing $\nu_r\theta_2$ by θ_2. Then there remains only one characteristic parameter, $A/A_0 = 2\pi(\nu_r - 1)A/\Delta r$, for each value of which one gets one of the curves of Fig. 7.

The fraction of particles, f_2, striking probe 2 is obtained by taking at each ordinate $(R_2 - R_1)/A$ the ratio of the phase width inside the curve to 2π radians. Finally the ordinates are multiplied by A/A_0 to yield the curves of Fig. 8, which shows $f_2(A/A_0)$ vs $(R_2 - R_1)/A_0$. From Fig. 8 one can predict probe shadows for all combinations of parameters so long as the probes are 120 deg apart and ν_r is not too different from unity. Another useful representation derived from Fig. 8, and shown in Fig. 9, gives the total shadow width vs. A_0 for various amplitudes A. The A_0 may be predicted easily from the dee voltage, rf particle phase, and ν_r. Figure 10 shows a prediction based

on computer calculations of A_0 for 130-MeV α-particles in the 88-inch cyclotron. The shape of the curves of Fig. 9 is worth noting: for $A_0 > A$, $A \approx \Delta R_s/3$, but for $A_0 < A$, A is increasingly greater than $\Delta R_s/3$. In other words, probe shadows become deceptively sharp when A_0 becomes small, which occurs at large radii.

Probe shadows measured here and interpreted in this way have indicated radial amplitudes of about 1/4 in. for the 88-inch cyclotron. This helps to explain our favorable deflector channel transmission efficiency (about 40%) and good external-beam quality

Footnote and Reference

*Work done under the auspices of the U. S. Atomic Energy Commission.

1. A. A. Garren, D. L. Judd, L. Smith, and H. A. Willax, Electrostatic Deflector Calculations for the Berkeley 88-Inch Cyclotron, Nucl. Instr. Methods 18, 19, 525 (1962).

Figure Captions

Fig. 1(a). Phases of beam particles vs. radius for a hypothetical case.

(b). Intensity on a probe vs radius for hypothetical case of Fig. 1(a).

Fig. 2(a). Beam intensity vs radius for various negative frequency shifts. Reference frequency f_0 = 12.538 Mc/sec, α particles, 130 MeV. Taken from measurements but cleaned up to remove contributions of H_2^+ and "spurium."

Fig. 2(b). Beam intensity vs radius for various positive frequency shifts. Reference frequency f_0 = 12.538 Mc/sec, α particles, 130 MeV.

Fig. 3. Phase history of 130 MeV α-particle beam as deduced from I vs R curves of Fig. 2.

Fig. 4. Change in $\sin\phi$ resulting from a 100-A decrease in each trim-coil power-supply current, a 100-A increase in main-coil current, and a 10-kc/sec decrease in frequency.

Fig. 5. Contribution to ν_z^2 [i.e., of $-(R/B(dB/dR)]$ from increase of each power-supply current by 100 A and the main-coil by 10 A. The ν_z^2 curve is a computer prediction based on a particular set of trim-coil settings (130 MeV α particles).

Fig. 6. Graphical construction to deduce fraction of beam hitting two shadowing probes for $\nu_r = 1.05$, $\theta_2 = 120°$, $\Delta r/A = 0.12$.

(R_1 = radius, upstream probe; R_2 = radius, downstream probe; θ_2 = azimuth, downstream probe; 0 = azimuth, upstream probe.)

1. Draw curve 1: $1 - \cos\phi$
2. Draw curve 2: $(R_2 - R_1)/A + [1 - \cos(\phi - \nu_r\theta_2)]$
3. From origin draw horizontal segment to left of length $\Delta = 2\pi(\nu_r - 1)$

Fig. 9. Probe shadow widths ΔR_s vs $A_o = \Delta r/2\pi(\nu_r - 1)$ for various amplitudes A. Length unit for ΔR_s, A, and A_o arbitrary.

Fig. 10. $A_o = \dfrac{\Delta R}{2\pi(\nu_r - 1)}$ vs radius in 88-inch cyclotron for 130-MeV α particles, 65 kV dee voltage. Based on computer predictions.

4. From end of Δ segment draw vertical segment of height $\Delta r/A$
5. Complete triangle to obtain angle $\alpha = \cot^{-1}(A\Delta/\Delta r)$
6. Mark intersections A, B of curves 1 and 2
7. Draw a line, parallel to OP, at angle α, as high as possible but not above intersection A or above curve 2
8. Draw a line, parallel to OP, at angle α, as high as possible but not above intersection B or above curve 1
9. Mark intersection P, A of the above two lines with abscissa OO'. Phases ϕ between ϕ_P and ϕ_Q (at turn zero) will strike probe 2. Hence fraction on probe 2 = $PQ/OO' = (\phi_Q - \phi_P)/360°$
10. Project P, Q upward onto horizontal line of height $(R_2 - R_1)/A$
11. Repeat procedure with new curves 2 for various $(R_2 - R_1)/A$. Connect resulting points P', Q'. The resulting curve (3) shows the phases hitting probe 2 as a function of radial probe separation.

Fig. 7. Radial oscillation phases striking shadowing probes. Each curve encloses phases striking $\begin{pmatrix}\text{downstream}\\ \text{upstream}\end{pmatrix}$ probe for $\nu_r \gtrless 1$. Ordinate is $\pm(R_2 - R_1)/A$ for $\nu_r \gtrless 1$.

Fig. 8. Shadow cast by one probe on another (separated by 120 deg) vs radial separation of the probes, for various radial amplitudes A.

$f = f_D$ = fraction of beam on downstream probe if $\nu_r > 1$

$f = f_U$ = fraction of beam on upstream probe if $\nu_r < 1$

R_D = radius of downstream probe

R_U = radius of upstream probe

$\Delta R_P = R_D - R_U$ if $\nu_r > 1$

$\Delta R_P = R_U - R_D$ if $\nu_r < 1$

$A_0 = \left|\dfrac{\Delta R}{2\pi(\nu_r - 1)}\right|$; ΔR = turn separation.

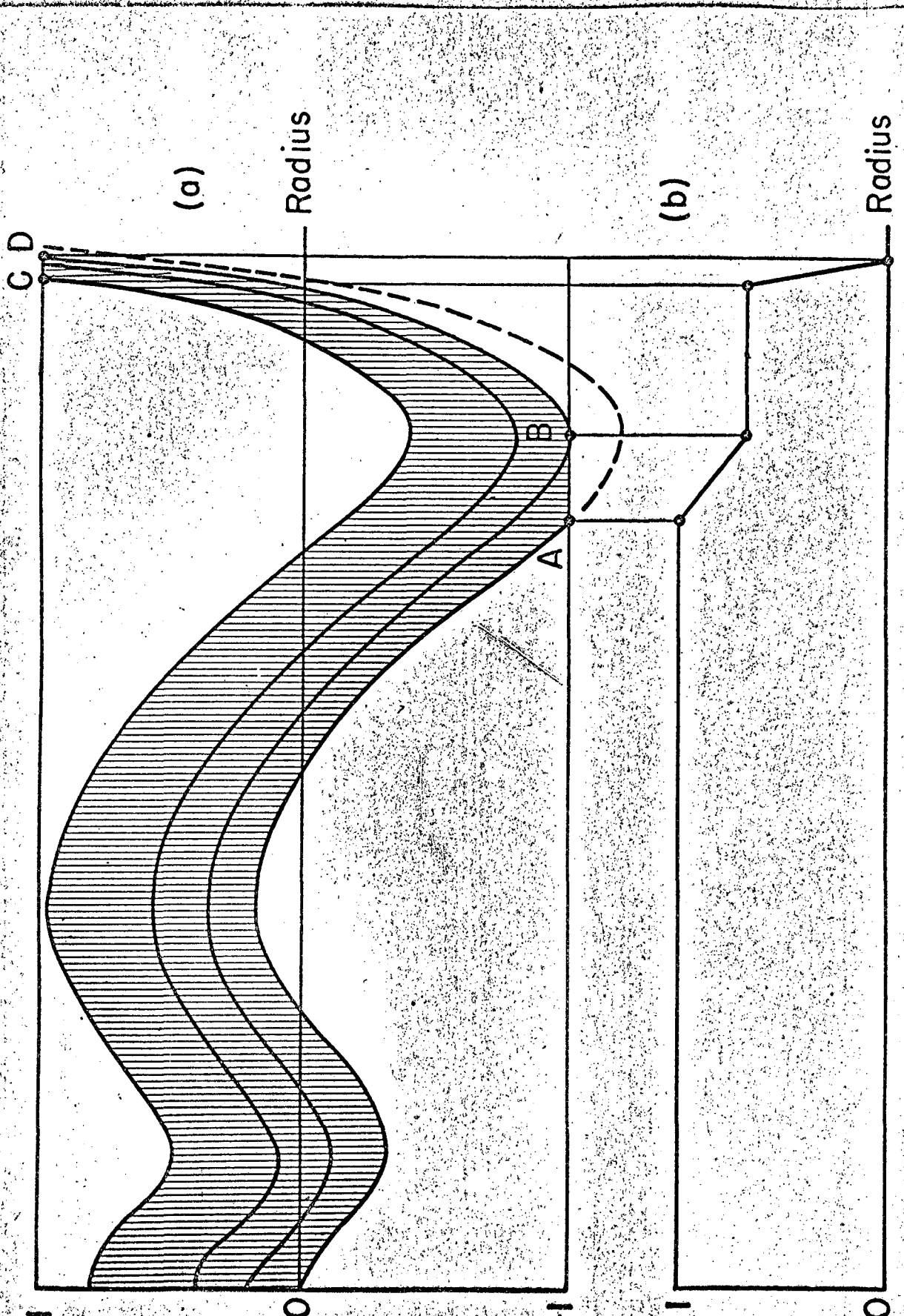

Fig. 1

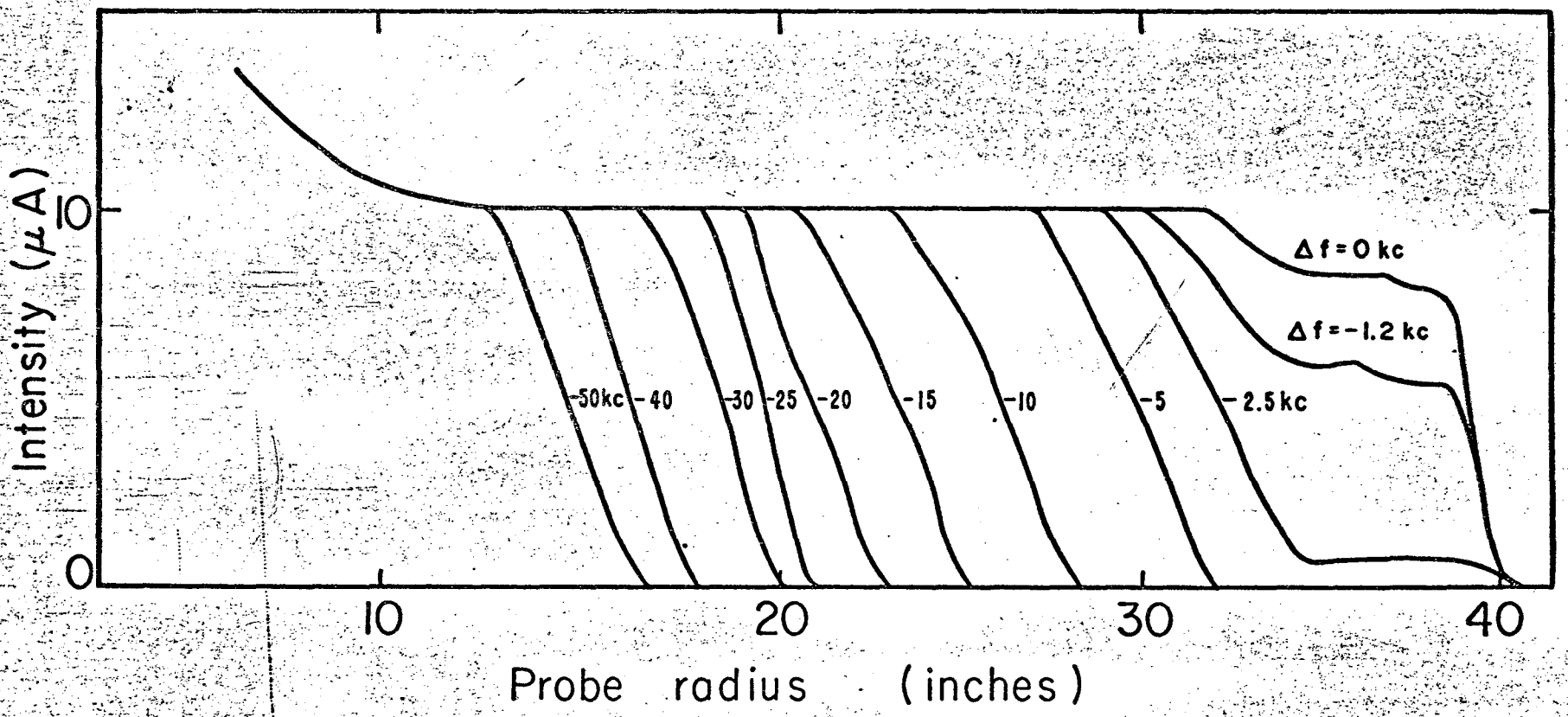
Intensity (μA)
10
0
10
20
30
40
Probe radius (inches)
Δf = 0 kc
Δf = -1.2 kc
-50kc
-40
-30
-25
-20
-15
-10
-5
-2.5kc
MU-30047

Fig. 2a

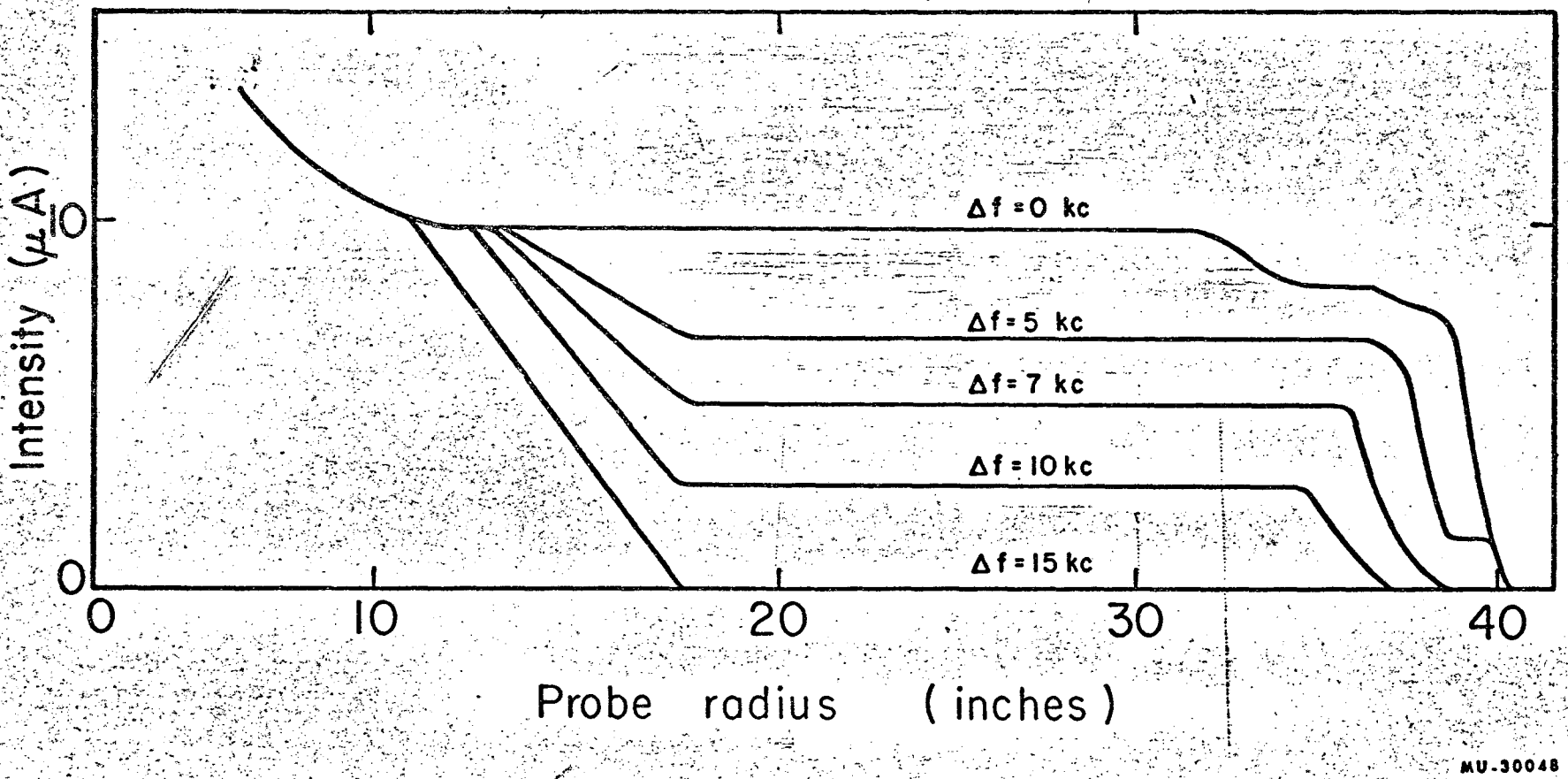
Intensity (μA)
10
0
Δf = 0 kc
Δf = 5 kc
Δf = 7 kc
Δf = 10 kc
Δf = 15 kc
0
10
20
30
40
Probe radius (inches)
MU-30048

Fig. 2b

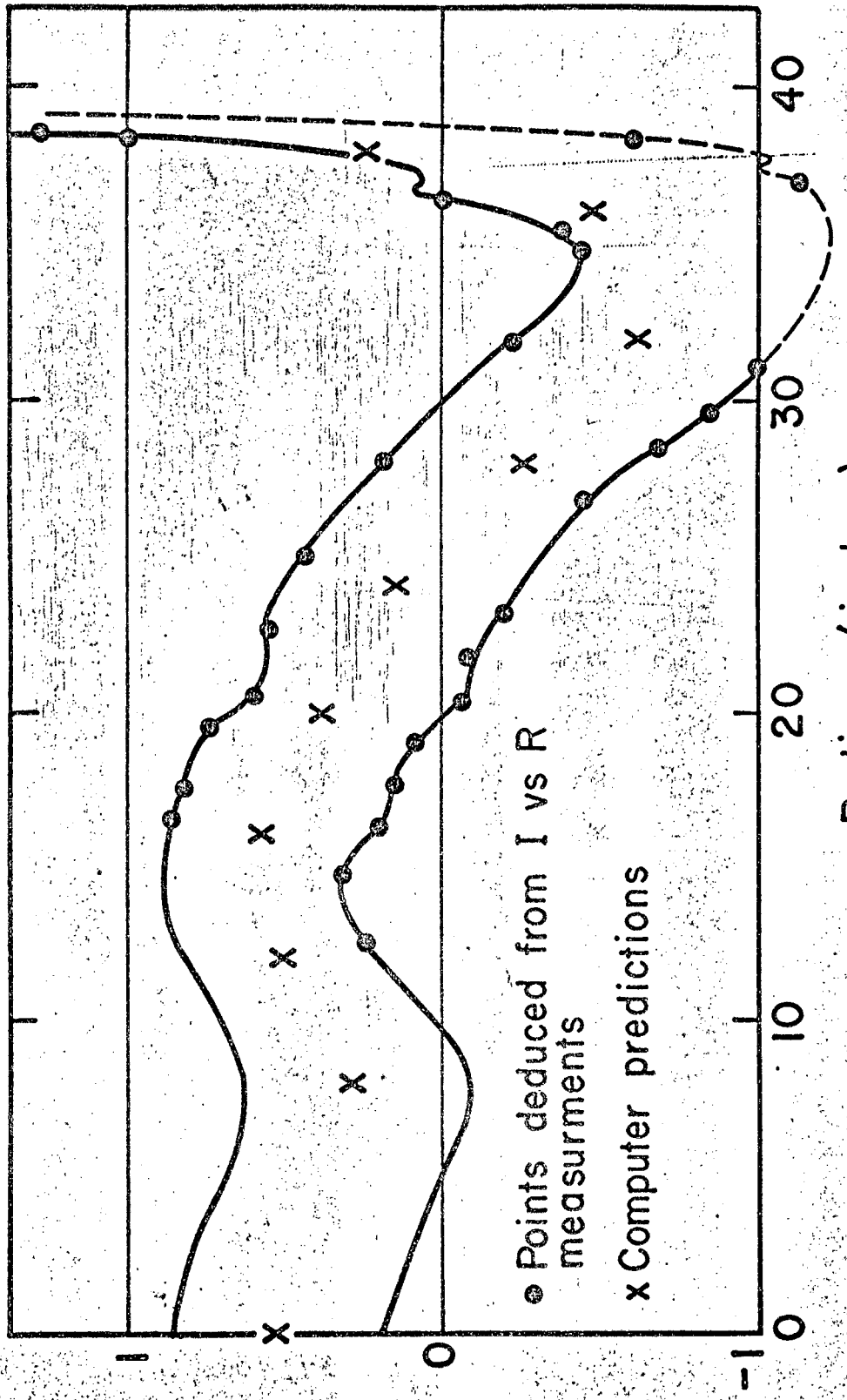
sin φ
1
0
-1
0
10
20
30
40
Radius (inches)
• Points deduced from I vs R measurments
x Computer predictions
MU-30049

Fig. 3

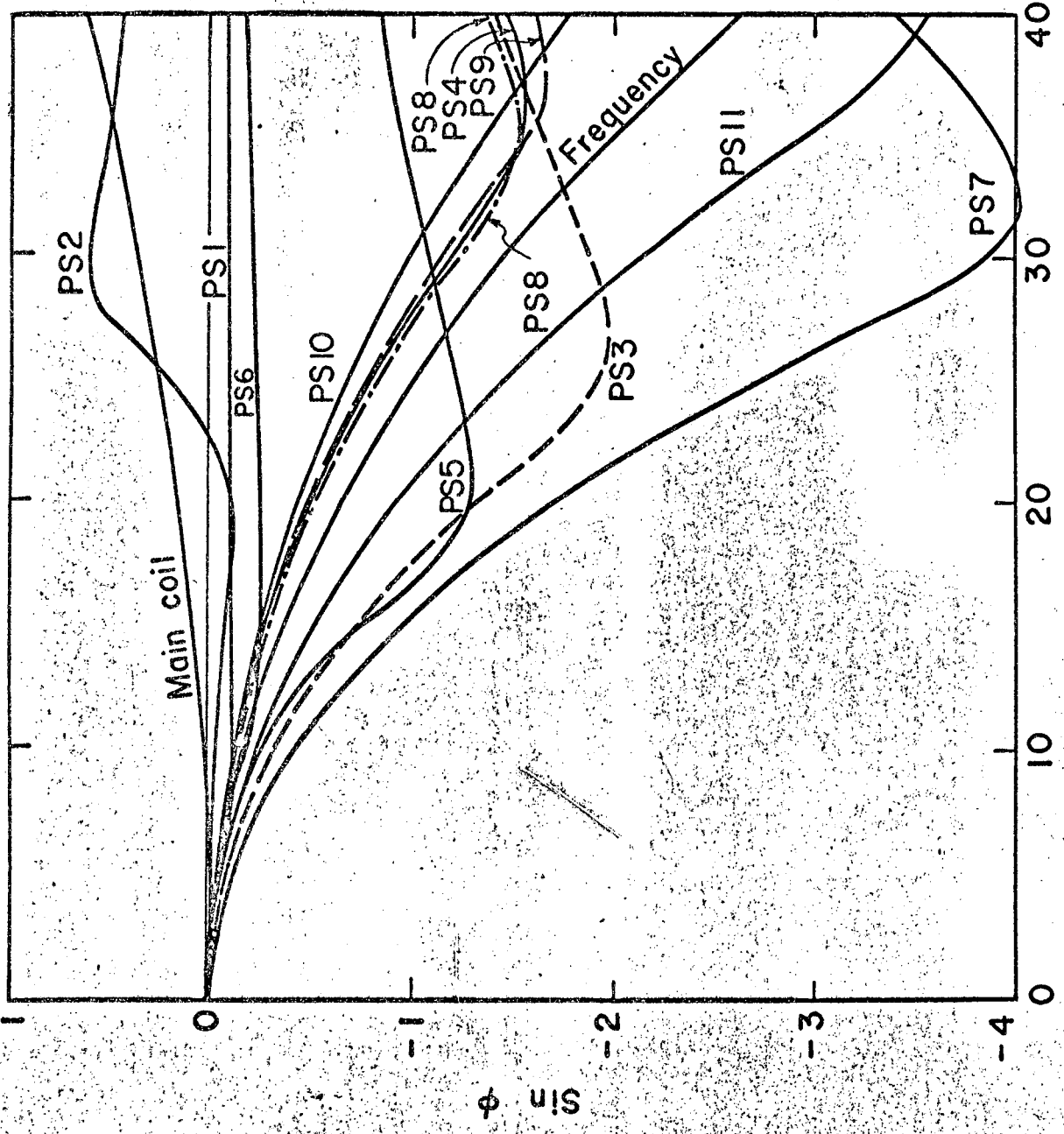

MUB-1694

Fig. 4

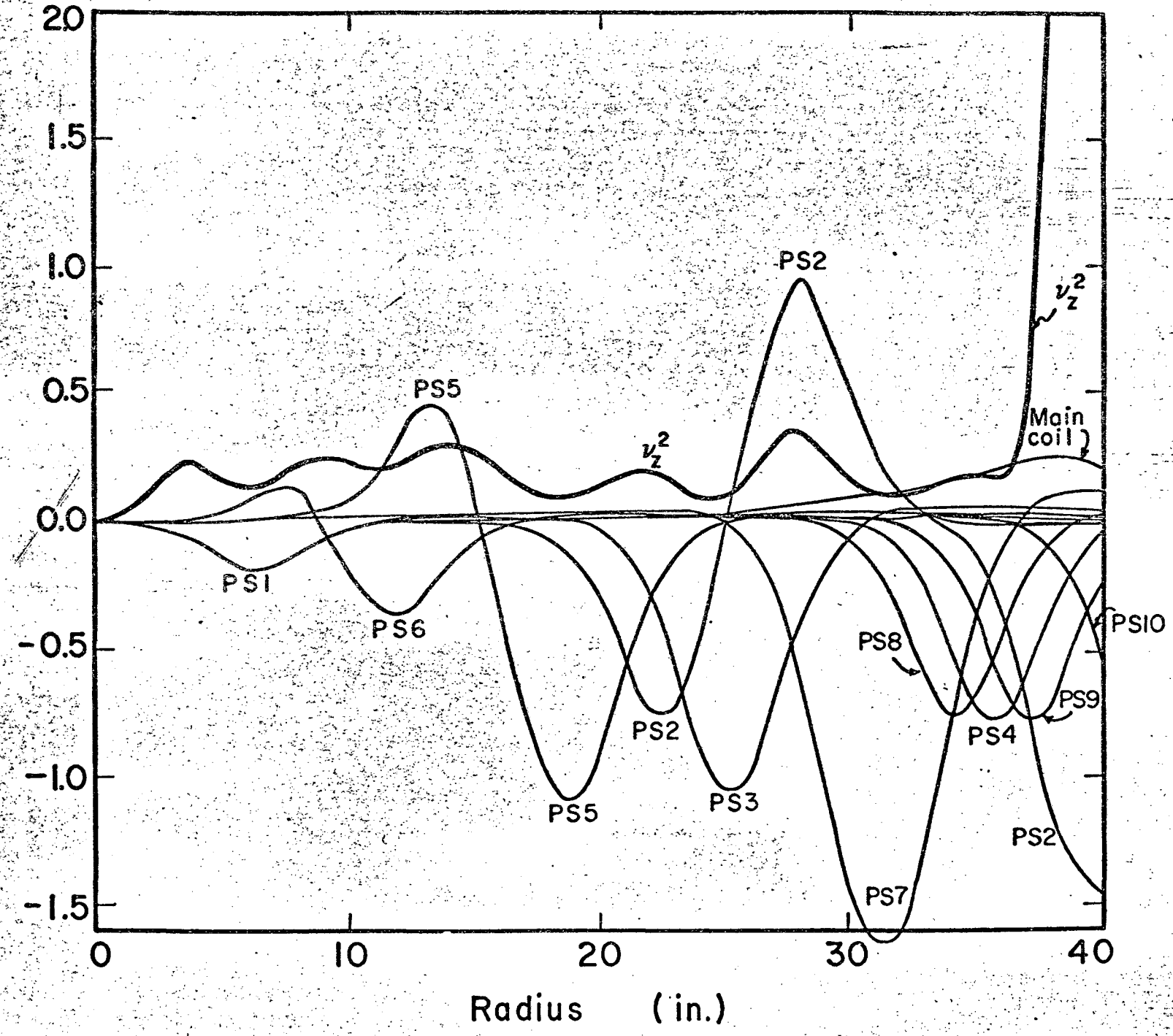

Fig. 5

MU-30050

UCRL-10756

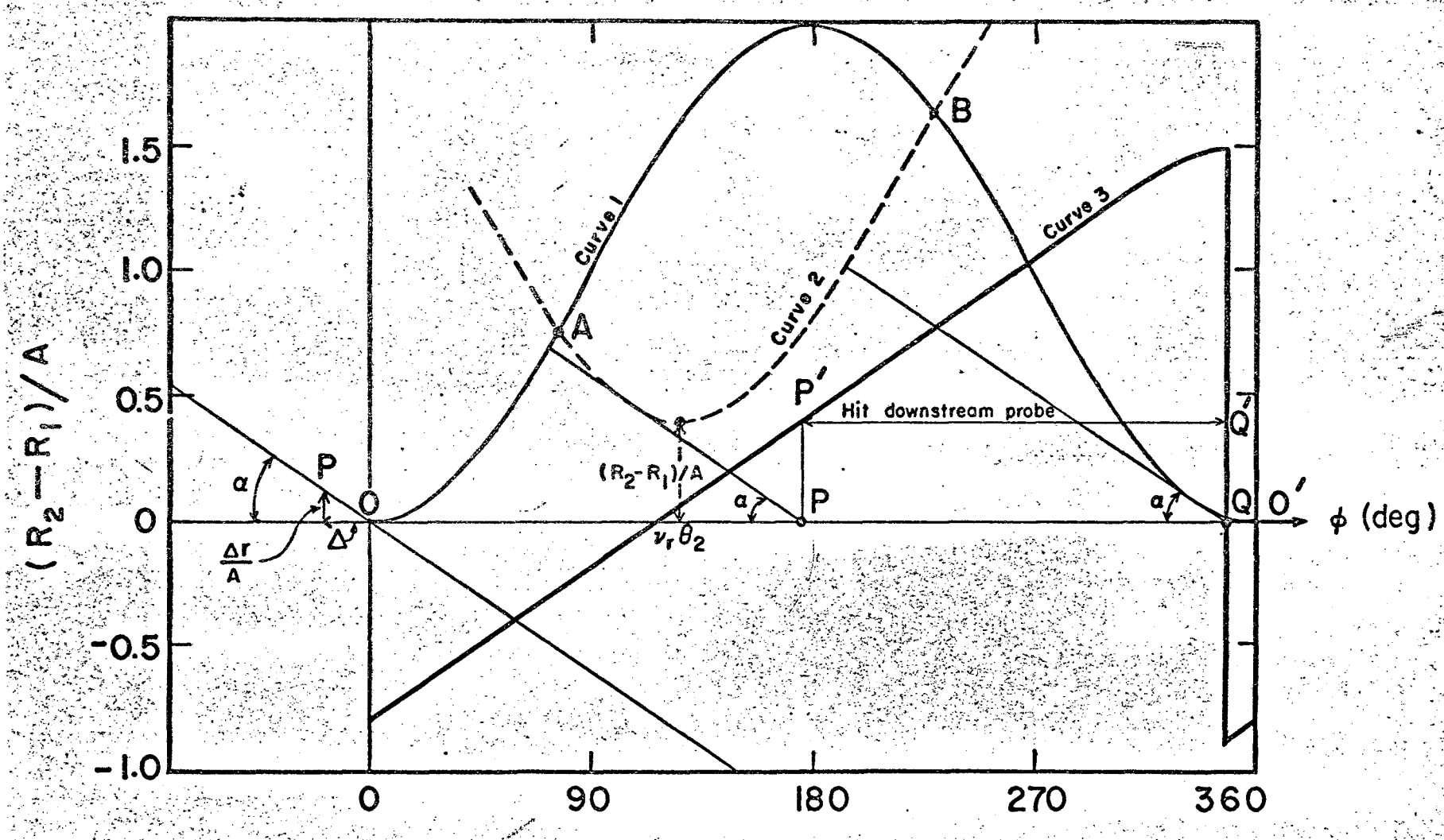

Fig. 6

UCRL-10756

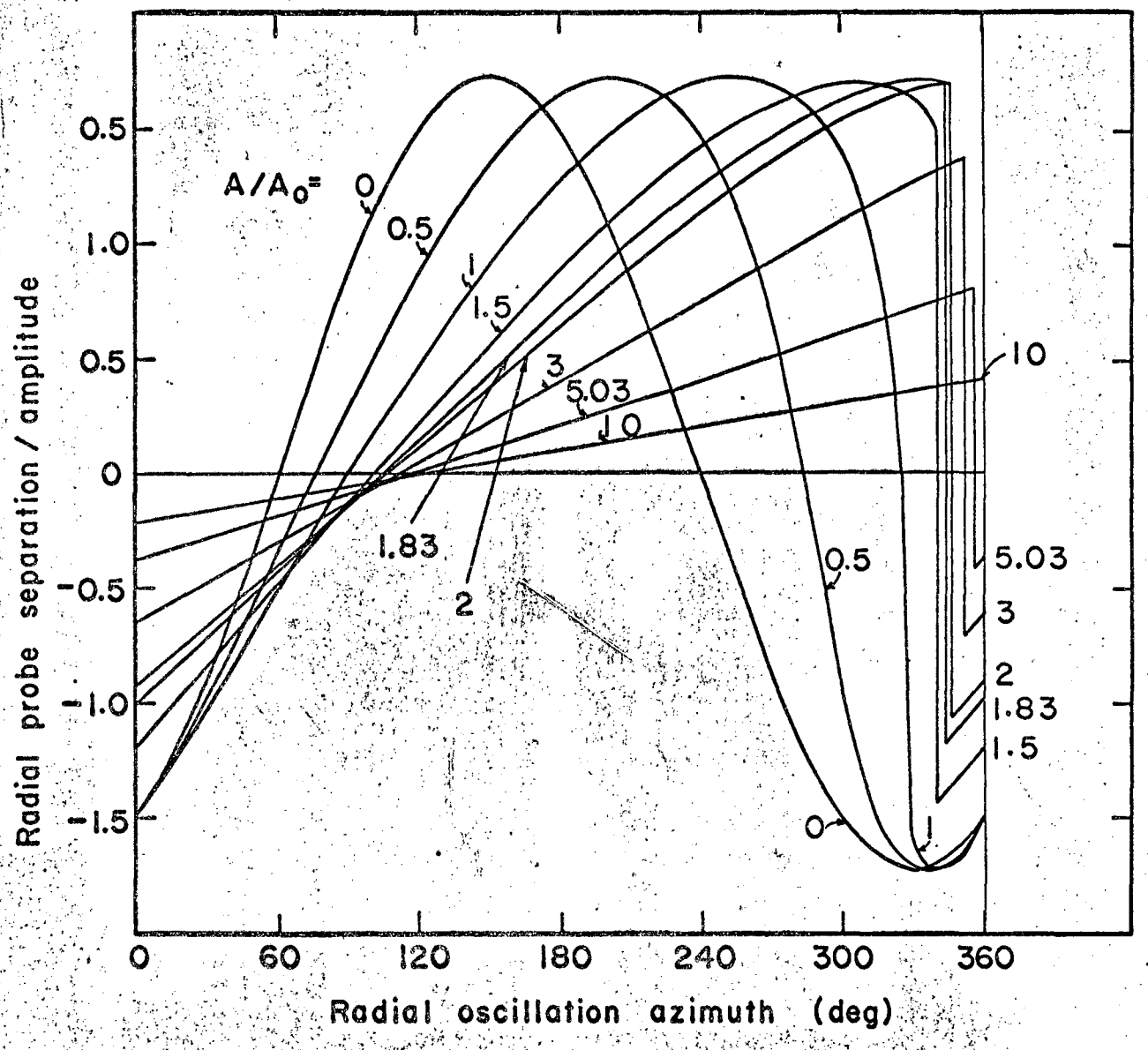

MUB-1693

Fig. 7

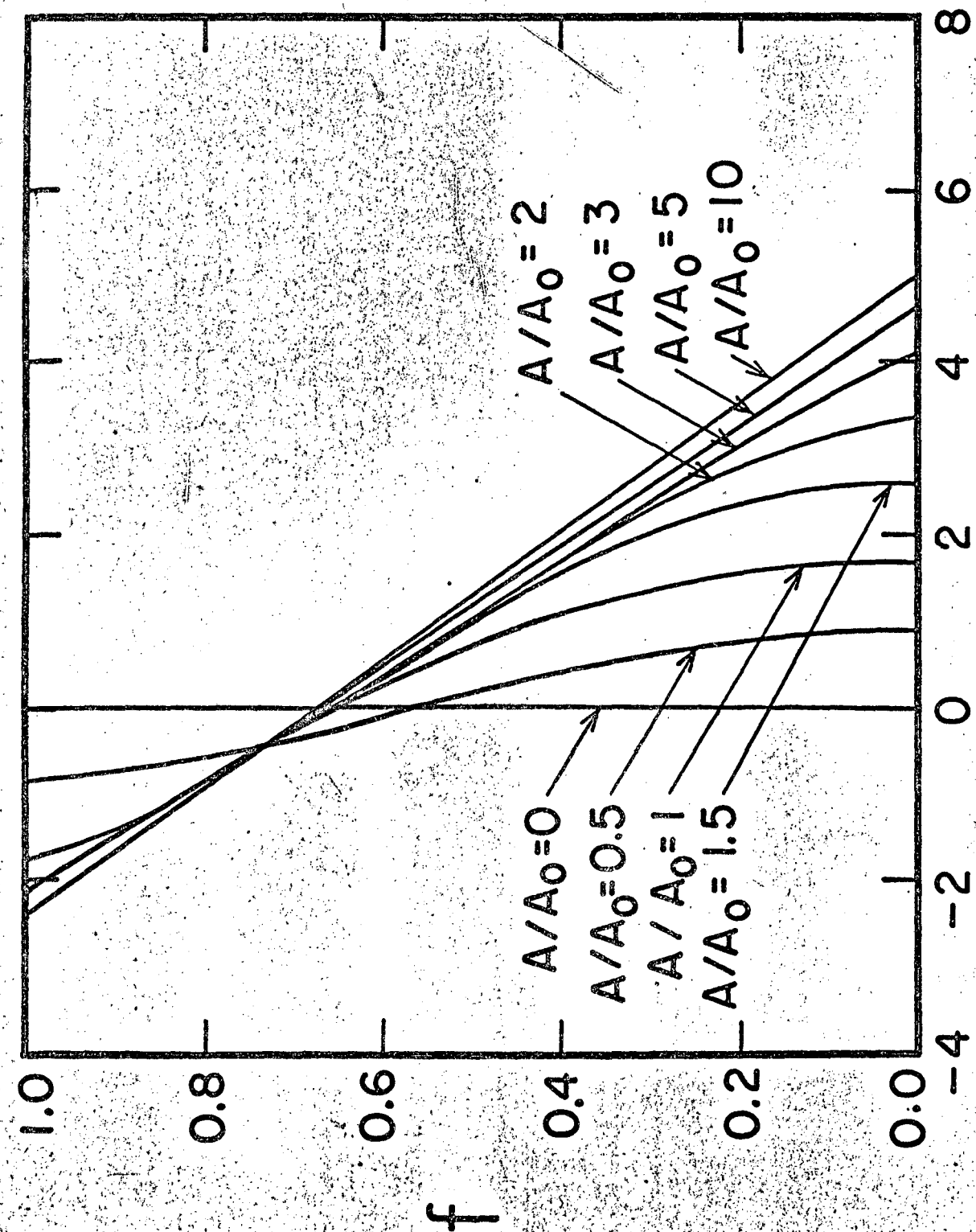

MU-30052

Fig. 8

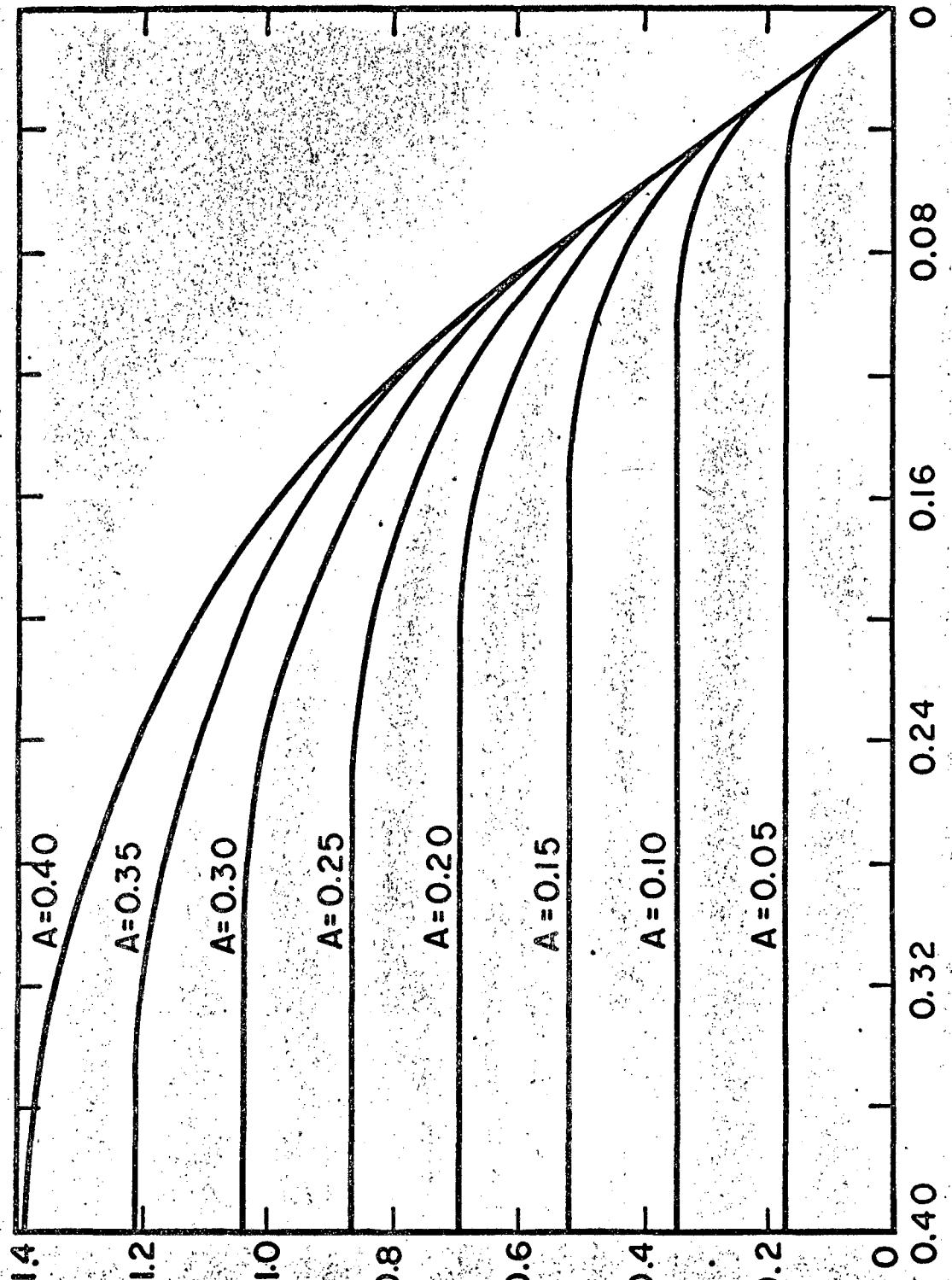
A=0.40
A=0.35
A=0.30
A=0.25
A=0.20
A=0.15
A=0.10
A=0.05
1.4
1.2
1.0
0.8
0.6
0.4
0.2
0
0.40
0.32
0.24
0.16
0.08
0
ΔR_s
A_0
MU-30053

Fig. 9